High-Efficiency Coupled-Inductor-Based Step-Down Converter

Rong-Jong Wai, *Senior Member, IEEE*, and Jun-Jie Liaw

***Abstract*—This study mainly investigates a high-efficiency single-input multiple-output (SIMO) step-down converter. The proposed converter can step down the voltage of a high-voltage dc bus generated by the rectifier of an ac utility power to a controllable low-voltage output terminal and middle-voltage output terminals. In this study, a coupled-inductor-based SIMO step-down converter utilizes two power switches with the properties of voltage clamping for the middle-voltage switch, and soft switching for all power switches due to the appropriate choice of the corresponding device specifications. As a result, the leakage inductor energy of the coupled inductor can be recycled, and the voltage spikes on power switches can be alleviated. Moreover, the switching losses can be significantly decreased because of all power switches with zero-voltage-switching features. Therefore, the objectives of high-efficiency power conversion, high step-down ratio, and various output voltage with different levels can be obtained. The effectiveness of the proposed SIMO step-down converter is verified by experimental results of a converter prototype in practical applications.**

***Index Terms*—Coupled inductor, high-efficiency power conversion, single-input multiple-output (SIMO), step-down converter, zero-voltage switching (ZVS).**

I. Introduction

In the past, the Kyoto Protocol implemented the objective of the climate change to fight global warming by reducing greenhouse gas concentrations in the atmosphere to a level. By accompanying the permission of Kyoto Protocol, clean energies, such as fuel cell (FC), photovoltaic (PV), and wind power, etc., have been rapidly promoted [1]–[4], wherein the wind power is one of efficient power generation systems. In the wind power generation system, its output power is easily influenced by environmental factors and wind intensity [5], [6]. According to these congenital limitations, the wind power generation system should have a battery module as an auxiliary backup power to be on standby. On the other hand, the auxiliary backup power from the battery module also has widely employed in uninterrupted power supplies (UPS) [7], [8]. In general, an ac utility power is used as the main power source for the UPS applications. Although the power conversion scheme with a step-down transformer plus a rectifier can produce a low-voltage dc source to charge the battery module, the output dc voltage cannot be arbitrarily adjusted, and its power conversion efficiency is degenerated. Recently, the diode rectifier with a buck converter has received much attention to cope with the control issue. However, increased switching loss and current stress are the critical drawbacks to be challenged. Besides, some peripheral devices with different voltage levels (e.g., microcontroller, cooling fan, etc.) should work well to ensure the proper operation before the wind power generation system or the UPS starts to produce power. The motivation of this study is to design a high-efficiency single-input multiple-output (SIMO) step-down converter for increasing the conversion efficiency, enhancing the voltage ratio, and possessing multiple output terminals with different voltage level.

Step-down converters with transformer-based structures are the most popular topologies [9]–[11], and soft-switching techniques are usually applied to reduce the corresponding switching losses. These frameworks with transformers have higher conduction losses because the number of power switches is usually over three. Nowadays, Gu *et al.* [12] proposed a family of switching capacitor regulators. Although only two power switches are required in [12], the values of the resonant capacitor and inductor should be strictly designed for ensuring all switches to be operated with the property of soft switching, and its framework is only suitable for one output terminal. Do [13] introduced a zero-voltage-switching (ZVS) synchronous buck converter with a coupled inductor. Unfortunately, this coupled inductor must have good matching characteristic to achieve the property of soft switching, and its voltage ratio is low. Lee [14] presented a new step-down converter scheme with an auxiliary switch, an auxiliary diode, and an auxiliary coupled winding to achieve the objective of high-efficiency power conversion under a wide range. But, two power switches and two diodes for only one output terminal are required so that the manufacturing cost is inevitably increased, and its voltage ratio is still low. Even though the step-down converters in [12]–[14] adopt the soft-switching techniques to minimize the corresponding switching losses, more power switches and passive components are always required so that the corresponding cost and volume will be inevitably increased. Hwu *et al.* [15] investigated an ultrahigh step-down converter, which combined one coupled inductor and one energy transferring capacitor. In [15], power switches were turned ON with near ZVS or ZVS due to blanking time, the leakage inductance, and the energy-transferring capacitor, without any additional components used. Although this topology has the same voltage gain as the proposed SIMO step-down converter in this study, three power switches are required for only

Manuscript received May 19, 2015; revised July 16, 2015; accepted August 16, 2015. Date of publication August 19, 2015; date of current version January 7, 2016. This work was supported in part by the Ministry of Science and Technology of Taiwan through Grant MOST 104-2221-E-011-172-MY3. Recommended for publication by Associate Editor D. Xu.

R. J. Wai is with the Department of Electronic and Computer Engineering, National Taiwan University of Science and Technology, Taipei 106, Taiwan (e-mail: rjwai@mail.ntust.edu.tw).

J. J. Liaw is with the Department of Electrical Engineering, Yuan Ze University, Chung Li 320, Taiwan (e-mail: s988503@mail.yzu.edu.tw).

Color versions of one or more of the figures in this paper are available online at http://ieeexplore.ieee.org.

Digital Object Identifier 10.1109/TPEL.2015.2470105

one output terminal, and there is no voltage clamping function within power switches.

As for the researches of interleaved step-down converters, Lee *et al.* [16] proposed an interleaved buck converter with low switching losses and improved step-down conversion ratio. Although the voltage stresses across power switches are half of the input voltage before turn-on or after turn-off when the operating duty is below 50%, the switching losses are still high due to the operation of hard switching, and its system control is more complicated. Pan *et al.* [17] presented a novel transformerless interleaved dc–dc converter with high step-down conversion ratio and low switch voltage stress. Although this converter adds two input capacitors as a voltage-divider circuit for increasing the step-down conversion ratio and reducing the voltage stresses of power switches, four power switches and two diodes are required so that the manufacturing cost is inevitably increased, and its control scheme is more complicated. For the multioutput application, Huang *et al.* [18] investigated a single-inductor dual-output buck converter. Although this converter can produce two different output voltages, the step-down conversion ratio is low, and its power conversion efficiency is degenerated due to the operation of hard switching. Wu *et al.* [19] performed the quasi two-stage architecture for the wide input voltage range and the high step-down multiple output conversion. Unfortunately, over two power switches for one output terminal are required.

In this study, a high-efficiency SIMO step-down converter with a coupled inductor is designed and implemented. The proposed converter uses two power switches to achieve the objectives of high-efficiency power conversion, high step-down ratio, and multiple output terminals with different voltage levels. In the proposed SIMO step-down converter, the techniques of soft switching is adopted to reduce the switching losses. Additionally, the problems of the stray inductance energy and reverse-recovery currents within diodes in the conventional step-down converter also can be solved. The output voltage range of the auxiliary circuit can be appropriately adjusted by the design of an auxiliary inductor. Wai and Jheng [20] developed a high-efficiency SIMO boost converter with the properties of voltage clamping and soft switching. The major difference between this study and [20] is the basic power conversion structure; i.e., the proposed circuit in this study is the buck-type converter framework, and the one in [20] is the boost-type converter circuit. Wai *et al.* [21] investigated the design of a high-efficiency bidirectional SIMO (BSIMO) power converter. In [21], three power switches (a low-voltage switch, a step-down switch, and a high-voltage switch), three inductors (a coupled inductor, an auxiliary inductor, and a step-down inductor), five capacitors (a clamped capacitor, a middle-voltage capacitor, and three filter capacitors), and four diodes were required. To compare with the proposed SIMO step-down converter including two power switches, two inductors, four capacitors, and two diodes, the circuit components of the low-voltage switch, the step-down inductor, the clamped capacitor, and two diodes in [21] can be saved. In other words, the proposed SIMO step-down converter has simpler circuit framework and lower manufacturing cost than the one in [21].

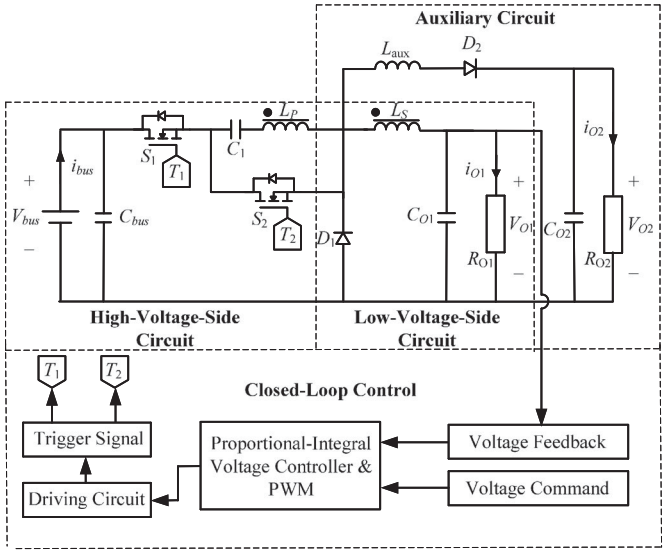

Fig. 1. System configuration of SIMO step-down converter.

II. Converter Design and Analyses

The system configuration for the proposed high-efficiency SIMO step-down converter topology is depicted in Fig. 1. This SIMO step-down converter contains three parts including a high-voltage-side circuit (HVSC), an auxiliary circuit, and a low-voltage-side circuit (LVSC). The major symbol representations are summarized as follows. $V_{\rm bus}$ ($i_{\rm bus}$) and V_{O1} (i_{O1}) denote the voltages (currents) of the input power source and the output terminal at the HVSC and LVSC, respectively; V_{O2} and i_{O2} are the output voltage and current in the auxiliary circuit. Note that, R_{O1} and R_{O2} are the equivalent loads in the LVSC and auxiliary circuit, respectively. $C_{\rm bus}$, C_{O1}, and C_{O2} are the filter capacitors at the HVSC, the LVSC, and the auxiliary circuit, respectively; C_1 is the middle-voltage capacitor in the HVSC. L_P and L_S represent individual inductors in the primary and secondary sides of the coupled inductor (T_r), respectively, where the primary side passed though the power switch (S_1) and the middle-voltage capacitor (C_1) is connected to the input power source; $L_{\rm aux}$ is the auxiliary inductor in the auxiliary circuit. S_1 and S_2 are the high-voltage switch and the middle-voltage switch, respectively.

The corresponding equivalent circuits used to define the voltage polarities and current directions are depicted in Fig. 2. The coupled inductor (T_r) in Fig. 1 can be modeled as an ideal transformer including the magnetizing inductor (L_{mp}) and the leakage inductor (L_{kp}) in Fig. 2. The turns ratio (N) and coupling coefficient (k_p) of this ideal transformer can be defined as

$$N = N_1/N_2 \tag{1}$$

$$k_p = L_{mp}/(L_{kp} + L_{mp}) = L_{mp}/L_P \tag{2}$$

where N_1 and N_2 are the winding turns in the primary and secondary sides of the coupled inductor (T_r). Because the voltage

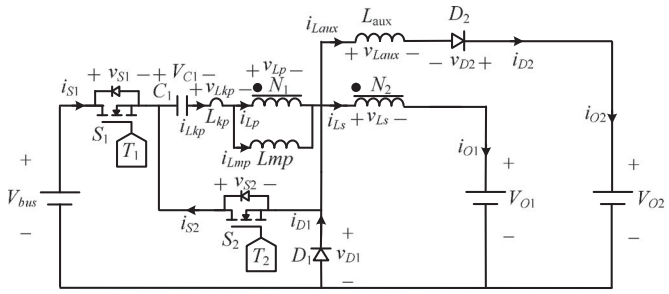

Fig. 2. Equivalent circuit of SIMO step-down converter.

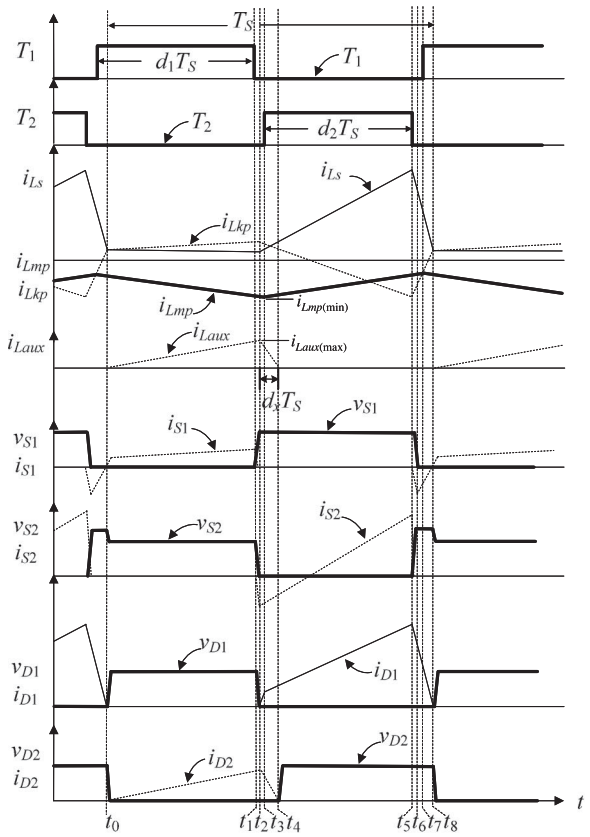

Fig. 3. Characteristic waveforms of SIMO step-down converter.

gain is less sensitive to the coupling coefficient, and the middle-voltage capacitor (C_1) is appropriately selected to absorb the leakage inductor energy [22], the coupling coefficient could be simply set at one ($k_p = 1$) to obtain $L_{mp} = L_P$ via (2). In this study, the assumption of the conduction voltage drops of the switches and diodes to be neglected is made to simplify the converter steady-state analyses.

The characteristic waveforms are depicted in Fig. 3, and the topological modes in one switching cycle are illustrated in Fig. 4. The driving signal (T_1) for the high-voltage switch (S_1) is complementary with the driving signal (T_2) for the middle-voltage switch (S_2). The duty cycles for the high-voltage switch (S_1) and the middle-voltage switch (S_2) are defined as d_1 and d_2, respectively. Moreover, T_S represents the switching period for power switches (S_1 and S_2).

A. Mode 1 ($t_0 - t_1$) [see Fig. 4(a)]

In this mode, the high-voltage switch (S_1) was turned ON, and the middle-voltage switch (S_2) was turned OFF for a span. The current (i_{S1}) from the HVSC passes through the middle-voltage capacitor (C_1), the primary winding (L_P), and the secondary winding (L_S). At the same time, partial energy of the primary winding (L_P) is transmitted to the auxiliary inductor ($L_{\rm aux}$). According to Kirchhoff's voltage law [23], the voltage $V_{\rm bus}$ can be given by

$$V_{\rm bus} = V_{C1} + v_{Lkp} + v_{Lp} + v_{Ls} + V_{O1}. \tag{3}$$

Because $v_{Lkp} = v_{Lp}(1 - k_p)/k_p$ and $v_{Ls} = v_{Lp}/N$, (3) can be rearranged as

$$\begin{aligned} V_{\rm bus} &= V_{C1} + v_{Lp}(1 - k_p)/k_p + v_{Lp} + v_{Ls} + V_{O1} \\ &= V_{C1} + v_{Lp}/k_p + v_{Lp}/N + V_{O1}. \end{aligned} \tag{4}$$

From (4), one can obtain

$$v_{Lp} = \frac{k_p N(V_{\rm bus} - V_{C1} - V_{O1})}{(N + k_p)}. \tag{5}$$

B. Mode 2 ($t_1 - t_2$) [see Fig. 4(b)]

At time $t = t_1$, the high-voltage switch (S_1) is turned OFF. The parasitic capacitor (c_{s2}) of the middle-voltage switch (S_2) starts to charge the middle-voltage capacitor (C_1) until the parasitic capacitor (c_{s2}) releases its stored energy completely. Then, the voltage across the middle-voltage switch (v_{S2}) resonates toward zero, and this mode ends.

C. Mode 3 ($t_2 - t_3$) [see Fig. 4(c)]

At time $t = t_2$, the body diode of the middle-voltage switch (S_2) conducts to carry the current (i_{Lkp}) because the leakage inductor (L_{kp}) has to release its stored energy persistently. Moreover, the diode (D_1) conducts to carry the secondary current (i_{Ls}) because the primary winding of the coupled inductor (T_r) has to release its stored energy persistently. At the same time, the auxiliary inductor ($L_{\rm aux}$) continuously releases its stored energy for the output terminal (V_{O2}) in the auxiliary circuit through the diode (D_2).

D. Mode 4 ($t_3 - t_4$) [see Fig. 4(d)]

This mode begins when the middle-voltage switch (S_2) is triggered. Because the body diode of the middle-voltage switch (S_2) has conducted in mode 3 (i.e., the voltage across the middle-voltage switch (S_2) is zero), the middle-voltage switch (S_2) is turned ON under the condition of ZVS, which is useful to reduce the switching loss in the HVSC. In this mode, the current (i_{Lkp}) continues to charge the middle-voltage capacitor (C_1), and the secondary winding (L_S) still provides the energy for the output terminal (V_{O1}) in the LVSC. Moreover, the auxiliary inductor ($L_{\rm aux}$) still release its stored energy for the output terminal (V_{O2})

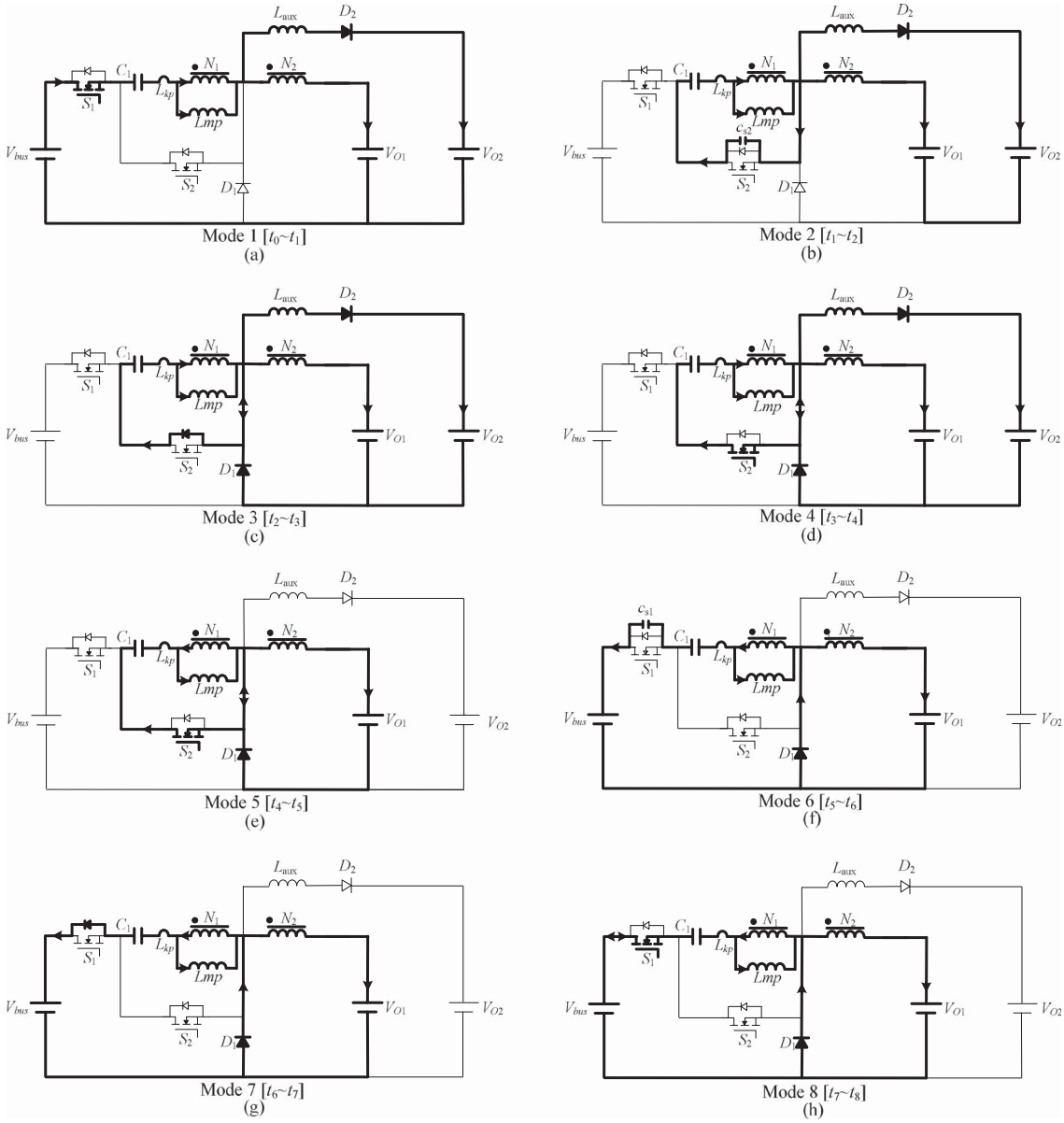

Fig. 4. Topological modes: (a) Mode 1 $[t_0 - t_1]$; (b) Mode 2 $[t_1 - t_2]$; (c) Mode 3 $[t_2 - t_3]$; (d) Mode 4 $[t_3 - t_4]$; (e) Mode 5 $[t_4 - t_5]$; (f) Mode 6 $[t_5 - t_6]$; (g) Mode 7 $[t_6 - t_7]$; (g) Mode 8 $[t_7 - t_8]$.

in the auxiliary circuit. When the auxiliary inductor current (i_{Laux}) drops to zero, this mode ends.

E. Mode 5 ($t_4 - t_5$) [see Fig. 4(e)]

At time $t = t_4$, the auxiliary inductor (L_{aux}) releases its stored energy completely, and the diode (D_2) turns OFF. At the same time, the current (i_{Lkp}) continues to charge the middle-voltage capacitor (C_1), and the secondary winding (L_S) still provides the energy for the output terminal (V_{O1}) in the LVSC. During the middle stage of this mode, the primary winding (L_P) releases its stored energy completely, and the primary current (i_{Lkp}) drops to zero. After that, the middle-voltage capacitor (C_1) starts to release its stored energy for the LVSC via the magnetic coupling way, and the primary magnetizing current (i_{Lmp}) via the flyback operational way induces the primary current (i_{Lkp}) magnetically to charge the middle-voltage capacitor (C_1). According to Kirchhoff's voltage law [23], the voltage (v_{Lp}) can be given by

$$v_{Lp} = -V_{C1}. \tag{6}$$

Moreover, the voltage (v_{Ls}) can be expressed as

$$v_{Ls} = -V_{O1} \tag{7}$$

According to (1) and (7), (6) can be rearranged as

$$v_{Lp} = N v_{LS} = -N V_{O1}. \tag{8}$$

Due to the relations of (6) and (8), the voltage across the middle-voltage capacitor (V_{C1}) can be represented as

$$V_{C1} = NV_{O1}. \tag{9}$$

F. Mode 6 ($t_5 - t_6$) [see Fig. 4(f)]

At time $t = t_5$, the middle-voltage switch (S_2) is turned OFF. The leakage inductor (L_{kp}) releases its stored energy into the middle-voltage capacitor (C_1), and the parasitic capacitor (c_{s1}) of the high-voltage switch (S_1) starts to release its stored energy for the input terminal ($V_{\rm bus}$) of the HVSC. Consequently, the polarities across the primary and secondary windings of the coupled inductor are reversed instantaneously because of $V_{\rm bus} > V_{O1}$. Because the secondary winding (L_S) still needs to release its energy for the output terminal (V_{O1}) in the LVSC, the diode (D_1) continuously conducts to sustain the sum of the currents (i_{Lkp} and i_{Ls}).

G. Mode 7 ($t_6 - t_7$) [see Fig. 4(g)]

At time $t = t_6$, the parasitic capacitor (c_{s1}) of the high-voltage switch (S_1) releases its stored energy completely. Because the leakage inductor (L_{kp}) still release its stored energy persistently, the body diode of the high-voltage switch (S_1) conducts to carry the current (i_{Lkp}).

H. Mode 8 ($t_7 - t_8$) [see Fig. 4(h)]

At time $t = t_7$, the high-voltage switch (S_1) is turned ON under the condition of ZVS because the body diode of the high-voltage switch (S_1) has conducted in mode 7. It provides a magnetizing path for the coupled inductor (T_r) so that the magnetizing inductor L_{mp} magnetizes again and the secondary current (i_{LS}) gradually decreases. According to the magnetizing effect of the primary winding, the nondotted point voltage of the secondary winding is negative. The diode (D_1) will turn OFF at time $t = t_8$ to complete one switching period. After that, it begins the next switching cycle and repeats the operation in mode 1.

The mode operation conditions are summarized as follows. In mode 1, the high-voltage switch (S_1) was turned ON, and the middle-voltage switch (S_2) was turned OFF for a span. When the high-voltage switch (S_1) is turned OFF, the operation enters mode 2. Moreover, the operation enters mode 3 when the body diode of the middle-voltage switch (S_2) conducts to carry the current (i_{Lkp}). Mode 4 begins when the middle-voltage switch (S_2) is triggered. When the auxiliary inductor ($L_{\rm aux}$) releases its stored energy completely, and the diode (D_2) turns OFF, the operation enters mode 5. Mode 6 starts when the middle-voltage switch (S_2) is turned OFF. In addition, the operation enters mode 7 when the body diode of the high-voltage switch (S_1) conducts to carry the current (i_{Lkp}). When the high-voltage switch (S_1) is turned ON under the condition of ZVS, the operation enters the mode 8. After the diode (D_1) turns OFF, it begins the next switching cycle and repeats the operation in mode 1.

The derivations of the voltage gain at the SIMO step-down converter are introduced as follows. For easy to analyze, the duty cycles for the high-voltage switches (S_1) and the middle-voltage switch (S_2) are defined as d_1, and d_2, respectively. At the SIMO step-down converter, d_2 is approximately equal to $1 - d_1$ by neglecting the dead time. Because the middle-voltage capacitor (C_1) can be appropriately selected to absorb the leakage inductor energy [22], the coupling coefficient (k_p) could be simply set at one. By using the voltage-second balance [23] of the magnetizing inductor (L_{mp}), one can obtain

$$\frac{N(V_{\rm bus} - V_{C1} - V_{O1})}{N+1} d_1 T_S + (-V_{C1})(1-d_1)T_S = 0. \tag{10}$$

According to (10), the voltage gain (G_{V1}) of the proposed SIMO step-down converter from the HVSC to the LVSC can be represented as

$$G_{V1} = V_{O1}/V_{\rm bus} = d_1/(N+1). \tag{11}$$

For calculating the discharge time of the auxiliary inductor at modes 3 and 4, the corresponding time interval can be denoted as $d_x T_S = (t_4 - t_2)$. At the mode 1, the auxiliary inductor voltage ($v_{L\rm aux}$) can be expressed as

$$v_{L\rm aux} = V_{\rm bus} - V_{C1} - v_{Lp} - V_{O2}. \tag{12}$$

According to (1), (9), and the relation of $v_{Ls} + V_{O1} = v_{\rm Laux} + V_{O2}$, (12) can be rearranged as

$$v_{L\rm aux} = \frac{V_{\rm bus} - (N+1)V_{O2}}{(N+1)}. \tag{13}$$

By using the voltage–second balance [23] of the auxiliary inductor voltage ($v_{L\rm aux}$), one can obtain

$$\frac{V_{\rm bus} - (N+1)V_{O2}}{(N+1)} d_1 T_S + (-V_{O2}) d_x T_S = 0. \tag{14}$$

From (14), the voltage gain (G_{V2}) of the proposed SIMO step-down converter from the HVSC to the output terminal (V_{O2}) in the auxiliary circuit can be rearranged as

$$G_{V2} = \frac{V_{O2}}{V_{\rm bus}} = \frac{d_1}{(N+1)(d_x + d_1)}. \tag{15}$$

As can be seen from Fig. 3, the average value of the diode current (i_{D2}) can be calculated as

$$i_{D2(\rm avg)} = \frac{1}{T_S}\left[\frac{1}{2} i_{L\rm aux(max)} d_1 T_S + \frac{1}{2} i_{L\rm aux(max)} d_x T_S\right] \tag{16}$$

where $i_{L\rm aux(max)}$ is the maximum current of the auxiliary inductor and can be expressed as

$$i_{L\rm aux(max)} = (V_{O2}/L_{\rm aux}) d_x T_S. \tag{17}$$

By substituting the aforementioned equation into (16), one can obtain

$$i_{D2(\rm avg)} = \frac{V_{O2}}{2L_{\rm aux}} d_x T_S (d_1 + d_x). \tag{18}$$

Because the average current of the diode (D_2) is equal to the current (i_{O2}), the current ($i_{D2(\rm avg)}$) can be represented as

$$i_{D2(\rm avg)} = V_{O2}/R_{O2}. \tag{19}$$

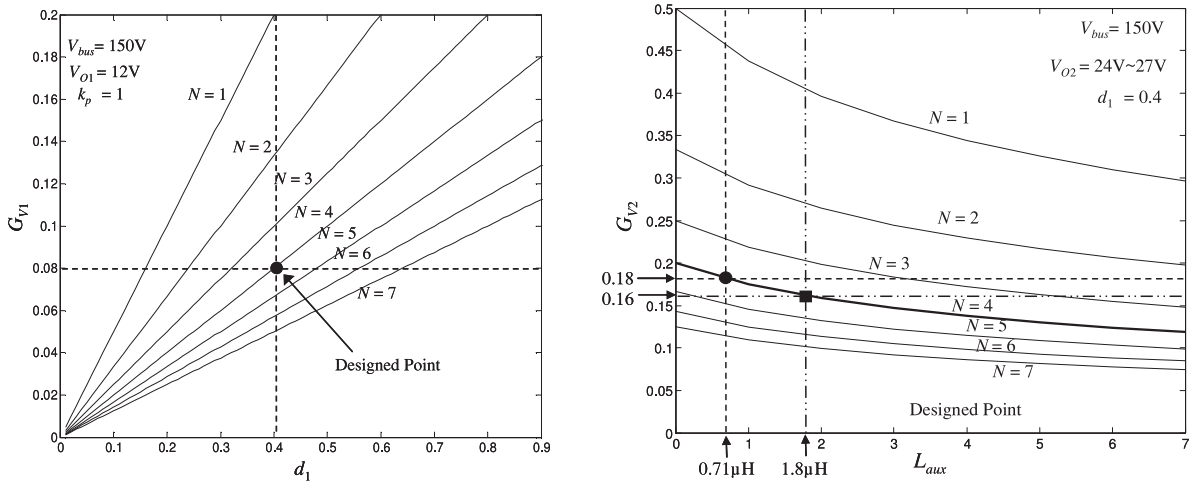

Fig. 5. (a) Voltage gain (G_{V1}) with respect to duty cycle (d_1) under different turns ratios; (b) voltage gain (G_{V2}) with respect to auxiliary inductors ($L_{\rm aux}$) under different turns ratios.

From (18) and (19), the duty cycle d_x can be rewritten as

$$d_x = \frac{-d_1 + \sqrt{d_1^2 + [8L_{\rm aux}/(R_{O2}T_S)]}}{2}. \tag{20}$$

The minimum magnetizing inductor current ($i_{Lmp(\min)}$) can be represented as

$$i_{Lmp(\min)} = i_{Lmp(\,\rm ave)} - \frac{\Delta i_{Lmp}}{2} \tag{21}$$

where $i_{Lmp(\,\rm ave)}$ and Δi_{Lmp} are the dc and ac components of i_{Lmp}. As can be seen from mode 4 or mode 5 in Figs. 3 and 4, the values of $i_{Lmp(\,\rm ave)}$ and Δi_{Lmp} can be calculated via (9) as

$$i_{Lmp(\,\rm ave)} = \frac{V_{O1}}{NR_{O1}} \tag{22}$$

$$\Delta i_{Lmp} = \frac{v_{Lmp}\Delta t}{L_{mp}} = \frac{V_{C1}(1-d_1)T_S}{L_{mp}} = \frac{NV_{O1}(1-d_1)T_S}{L_{mp}}. \tag{23}$$

According to (22) and (23), (21) can be rearranged as

$$i_{Lmp(\min)} = \frac{V_{O1}}{NR_{O1}} - \frac{NV_{O1}(1-d_1)T_S}{2L_{mp}}. \tag{24}$$

By considering the boundary condition of continuous and discontinuous magnetizing inductor current, the minimum magnetizing inductor ($L_{mp(\rm mim)}$) under continuous conduction mode (CCM) can be obtained as

$$L_{mp(\min)} \geq \frac{N^2R_{O1}(1-d_1)T_S}{2}. \tag{25}$$

In this study, the value of the magnetizing inductor (L_{mp}) should be selected over $L_{mp(\rm mim)}$ for ensuring the property of CCM according to (25).

III. Design Considerations

To verify the effectiveness of the proposed high-efficiency SIMO step-down converter topology, a 150-V power supply is utilized for the input power source ($V_{\rm bus}$) in the HVSC to imitate the rectifier of an utility power with the ac voltage 110 $V_{\rm rms}$, and the desired output dc voltage is set at 12 V in the LVSC. The maximum load current at the LVSC is set at 48 A, and its equivalent load in the LVSC is $R_{O1} = 0.25\,\Omega$. In the proposed SIMO step-down converter, a 24-V battery module is considered as the load in the auxiliary circuit. The maximum battery floating charge voltage is set at $V_{O2(\max)} = 27\,\rm V$, and the allowable charging power is 100 W ($R_{O2} = 7.2\,\Omega$). In addition, this converter is operated with a 100-kHz switching frequency ($f_s = 100\,\rm kHz$), and the coupling coefficient could be simply set at one ($k_p = 1$) because the proposed circuit has a good leakage energy recycling effect.

A. Determination of Duty Cycle and Turns Ratio

By substituting $N = 1 \sim 7$ into (11), the curves of the voltage gain G_{V1} with respect to different duty cycles (d_1) are depicted in Fig. 5(a). By analyzing Fig. 5(a), the turns ratio (N) of the coupled inductor can be selected as $N = 4$ when the operational conditions are $V_{\rm bus} = 150\,\rm V$ and $V_{O1} = 12\,\rm V$ (i.e., $G_{V1} = 0.08$) so that the corresponding duty cycle (d_1) can be obtained as $d_1 = 0.4$. According to (15), one can calculate the discharge duty cycle of the auxiliary inductor as $d_x = 0.04$ by using the values of $V_{\rm bus} = 150\,\rm V$, $N = 4$, $d_1 = 0.4$, and $V_{O2(\max)} = 27\,\rm V$.

B. Switch Voltage Stress Design

As can be seen from Figs. 3 and 4, the high-voltage switch (S_1) and the middle-voltage switch (S_2) are not turned ON simultaneously. The maximum voltage across the high-voltage switch (S_1) and the middle-voltage switch (S_2) can be

represented as

$$v_{S1,S2(\max)} = V_{\rm bus}. \tag{26}$$

Because the voltage across the middle-voltage switch (S_2) at the mode 1 can be represented as $v_{S2} = V_{C1} + v_{Lp}$. Due to the relations of (5) and (9), the voltage across the middle-voltage switch (S_2) at the mode 1 can be expressed as

$$v_{S2} = NV_{\rm bus}/(N+1). \tag{27}$$

According to the design of $V_{\rm bus} = 150\,{\rm V}$ and $N = 4$, the voltage of the middle-voltage switch (S_2) can be steadily clamped at 120 V. By analyzing (26) and (27), the maximum voltage across the high-voltage switch (S_1) and the middle-voltage switch (S_2) are not related to the duty cycles (d_1 and d_2) if the value of the high dc-bus voltage ($V_{\rm bus}$) and the turns ratio (N) are fixed. Due to the maximum voltage stress of $v_{S1,S2(\max)} = V_{\rm bus}$ and the possible occurrence of the circuit stray effect, the switches (S_1 and S_2) with 200-V voltage rating can be selected.

C. Diode Selection

In this study, the voltage across the diode (D_1) at the mode 1 can be expressed as $v_{D1} = V_{\rm bus} - [NV_{\rm bus}/(N+1)] = 30\,{\rm V}$ via $V_{\rm bus} = 150\,{\rm V}$ and $N = 4$. During the mode 5, the diode (D_2) turns OFF, and its voltage can be represented by $v_{D2} = V_{O2} + [L_{\rm aux}(di_{L\rm aux}/dt)]$. Since the auxiliary inductor current ($i_{L\rm aux}$) is equal to zero at the mode 5, the voltage (v_{D2}) can be rearranged as $v_{D2} = V_{O2} = 24\,{\rm V}$ by considering $V_{O2} = 24\,{\rm V}$. Thus, low-voltage Schottky diodes can be selected for the diodes (D_1 and D_2) to avoid the problem of reverse-recovery currents. In this study, the diode of Schottky Barrier Rectifiers MBR20200CT is selected for D_2. Because the diode (D_1) in the LVSC has a quite large current flowing through, the conduction loss should be specially considered to select the diode with low forward voltage for reducing the conduction loss. The conduction loss of D_1 can be calculated as $P_{D1,\rm loss} = i_{D1(\rm avg)}V_F$, in which $i_{D1(\rm avg)}$ and V_F are the average current and forward voltage of D_1, respectively. In this study, the diode of Schottky Rectifiers 60CPQ150 is selected for D_1. The forward voltage of D_1 is 0.67 V, which is smaller than the 0.9-V forward voltage of a general diode.

D. Coupled Inductor/Auxiliary Inductor Design

In this study, the rated output current at the LVSC (i_{O1}) is set at 45 A, and the corresponding output current of the LVSC at the minimum load is set at 10% of the rated load current at the LVSC, i.e., 4.5 A. As can be seen from mode 3 to mode 8 in Fig. 4, the current and voltage relation of the secondary winding (L_S) can be approximately represented as $v_{Ls} = L_S(\Delta i_{O1}/\Delta t)$. When one considers the predetermined values of $v_{Ls} = 12\,{\rm V}$ and $\Delta t = (1-d_1)T_S = 6\,\mu{\rm s}$, and the maximum variation of $\Delta i_{O1} = 45\,{\rm A} - 4.5\,{\rm A} = 40.5\,{\rm A}$, the value of $L_S = 1.78\,\mu{\rm H}$ can be calculated. In order to manufacture the inductor easily, the value of $L_S = 2\,\mu{\rm H}$ is adopted in the experimental prototype. Because the ratio of the primary and secondary inductors in the coupled inductor (T_r) is square proportional to the turns ratio ($N = 4$), the value of L_P can be determined as $32\,\mu{\rm H}$. The selection of $L_P = 32\,\mu{\rm H}$ satisfies the condition in (25) for ensuring the property of CCM.

By substituting (20) into (15), the voltage gain (G_{V2}) of the proposed SIMO step-down converter from the HVSC to the output terminal (V_{O2}) in the auxiliary circuit can be rearranged as

$$G_{V2} = \frac{V_{O2}}{V_{\rm bus}} = \frac{2d_1}{(N+1)(d_1 + \sqrt{d_1^2 + [8L_{\rm aux}/(R_{O2}T_S)]})}. \tag{28}$$

As can be seen from (28), the voltage of the output terminal (V_{O2}) in the auxiliary circuit can be appropriately regulated by the design of the auxiliary inductor (L_{aux}) when the voltage of the HVSC ($V_{\rm bus}$), the turns ratio (N), the duty cycle (d_1), the switching cycle (T_S), and the equivalent load (R_{O2}) are determined in advance. By substituting $N = 1 \sim 7$, $d_1 = 0.4$, $R_{O2} = 7.2\,\Omega$, and $T_S = 10\mu{\rm s}$ into (28), the curves of the voltage gain (G_{V2}) with respect to different auxiliary inductors ($L_{\rm aux}$) are depicted in Fig. 5(b). By considering $N = 4$, $V_{\rm bus} = 150\,{\rm V}$, and $V_{O2} = 24\,{\rm V} \sim 27\,{\rm V}$ (i.e., $G_{V2} = 0.16 \sim 0.18$), the upper and lower values of the auxiliary inductor can be obtained between 0.71 and 1.8 μH from Fig. 5(b). In this study, its average value $L_{\rm aux} = 1.3\,\mu{\rm H}$ is adopted.

E. Filter Capacitor/ Energy-Transferring Capacitor Design

In the proposed SIMO step-down converter, the electric charge variation (ΔQ_{O2}) of the filter capacitor (C_{O2}) in the auxiliary circuit can be represented as $\Delta Q_{O2} = (V_{O2}/R_{O2})(d_1 - d_x)T_S = C_{O2}\Delta V_{O2}$, and the voltage ripple of V_{O2} can be rearranged as $(\Delta V_{O2}/V_{O2}) = (d_1 - d_x)/(R_{O2}C_{O2}f_S)$. By substituting $d_1 = 0.4$, $G_{V2} = 0.18$, and $N = 4$ into (15), the duty cycle d_x can be calculated as 0.04. If one sets the voltage ripple of V_{O2} to be less than 1%, the value of C_{O2} should be selected over $50\mu{\rm F}$ by substituting $d_1 = 0.4$, $d_x = 0.04$, $R_{O2} = 7.2\,\Omega$, $f_S = 100\,{\rm kHz}$, and $V_{O2} = 27\,{\rm V}$ into the function of $C_{O2} = (d_1 - d_x)/[(R_{O2}f_S)(\Delta V_{O2}/V_{O2})]$. Moreover, the electric charge variation (ΔQ_{O1}) of the filter capacitor (C_{O1}) in the LVSC can be expressed as $\Delta Q_{O1} = (V_{O1}/R_{O1})(1 - d_1)T_S = C_{O1}\Delta V_{O1}$, and the ripple of the output voltage (V_{O1}) can be rearranged as $(\Delta V_{O1}/V_{O1}) = (1 - d_1)/(R_{O1}C_{O1}f_S)$. By substituting $f_S = 100{\rm kHz}$, $d_1 = 0.4$, $R_{O1} = 0.25\,\Omega$, and $V_{O1} = 12\,{\rm V}$ into the function of $C_{O1} = (1 - d_1)/[(R_{O1}f_S)(\Delta V_{O1}/V_{O1})]$, the value of C_{O1} should be chosen over $2400\,\mu{\rm F}$ with the constraint on the voltage ripple to be less than 1%. According to the aforementioned consideration, the values of $C_{O1} = 2400\,\mu{\rm F}$ and $C_{O2} = 50\mu\,{\rm F}$ are adopted in the experimental prototype.

The middle-voltage capacitor (C_1) is used to transfer the energy from the input to the output including the leakage inductor energy. Thus, the capacitance of C_1 can be estimated by the following equation:

$$C_1 > 2P_{O1,\rm rated}/(V_{C1}^2 f_S) \tag{29}$$

where $P_{O1,\rm rated}$ is the rated output power of the LVSC. According to (9), (29) can be rewritten as

$$C_1 > \frac{2P_{O1,\rm rated}}{(NV_{O1})^2 f_S}. \tag{30}$$

By substituting $N = 4$, $V_{O1} = 12\,\text{V}$, $f_s = 100\,\text{kHz}$, and $P_{O1,\text{rated}} = 540\,\text{W}(V_{O1} = 12\,\text{V}$ and $i_{O1} = 45\,\text{A})$ into (30), one can obtain $C_1 > 4.69\,\mu\text{F}$. Because the value of C_1 should be larger enough to avoid resonance with the leakage inductor [24], one selects the middle-voltage capacitor as $C_1 = 10\,\mu\text{F}$ in this study.

F. Feedback Control Design

In this study, the feedback control is used to solve the problem of the output voltage varied with load variations, and a digital-signal-processor (DSP) TMS320F2812 manufactured by Texas Instruments is adopted to achieve this goal of feedback control. In this feedback scheme, conventional proportional-integral (PI) control without detailed mathematical dynamic model is utilized. In this study, the output voltage (V_{O1}) of the LVSC is controllable via a conventional PI control framework, and the voltage level of the output voltage (V_{O2}) in the auxiliary circuit is regulated by the design of the auxiliary inductor (L_{aux}). Although the voltage of the output terminal in the auxiliary circuit cannot be precisely controlled real time, the predetermined voltage range by the design of the auxiliary inductor (L_{aux}) is suitable for the floating charge voltage to a battery module as the load in the auxiliary circuit.

IV. Experimental Results

A prototype with the following specifications is first designed in this section to verify the design procedure given in Section III.

Input voltage for HVSC	$V_{\text{bus}} = 150\,\text{V}$.
Output voltage for LVSC	$V_{O1} = 12\,\text{V}$.
Auxiliary output voltage	$V_{O2} = 24\,\text{V} - 27\,\text{V}$.
Switching frequency	$f_S = 100\,\text{kHz}$.
Coupled inductor	$L_P = 32\,\mu\text{H}$; $L_S = 2\,\mu\text{H}$; $N = 4$; $k_p = 0.95$; EE-55 core.
Switch	S_1, S_2: IRFP260N (200 V/50 A $\times$ 2, $R_{\text{DS(on)}} = 40\,\text{m}\Omega$); TO-247AC.
Diode	D_1: Schottky Rectifiers 60CPQ 150, (150 V/60 A $\times$ 2, $V_F = 0.67$). D_2: Schottky Barrier Rectifiers MBR20200CT, (200 V/20 A, $V_F = 0.9$).
Inductor	$L_{\text{aux}} = 1.3\,\mu\text{H}$.
Capacitor	$C_1 = 10\,\mu\text{F}/250\,\text{V}$. $C_{O1} = 2400\,\mu\text{F}/35\,\text{V}$; $C_{O2} = 50\,\mu\text{F}/60\,\text{V}$.

Note that, a battery with the electric specification of 12 V and 55 Ah, manufactured by the GS Battery Company, is adopted and two batteries are connected in series to take as the output load in the auxiliary circuit. The use of battery in the auxiliary circuit is just an example for the equivalent load R_{O2} in Fig. 1, not a power-supply source for the proposed high-efficiency SIMO step-down converter. Even for two different voltages in parallel, no large circulating current will occur because of the directional diode of D_2 and the design of $V_{O2} > V_{O1}$. In real applications, the battery module in the auxiliary circuit can supply its power for other peripheral devices, for example, an electronic control board, a cooling fan, etc. Although the voltage of the middle-voltage output terminal (V_{O2}) is incontrollable real time, the predetermined voltage range by the design of the auxiliary inductor (L_{aux}) is suitable for the floating charge voltage to a battery module as the load in the auxiliary circuit. As long as the voltage of the middle-voltage output terminal (V_{O2}) is larger than the voltage of the battery module, one can use the floating charge way to charge the battery module. The auxiliary battery module used in this study also can be extended easily to other dc loads, even for different voltage demands, via the manipulation of circuit components design. The practical photograph of the proposed SIMO step-down converter is depicted in Fig. 6, where the front side and the reverse side of the converter prototype are given in Fig. 6(a) and (b), respectively.

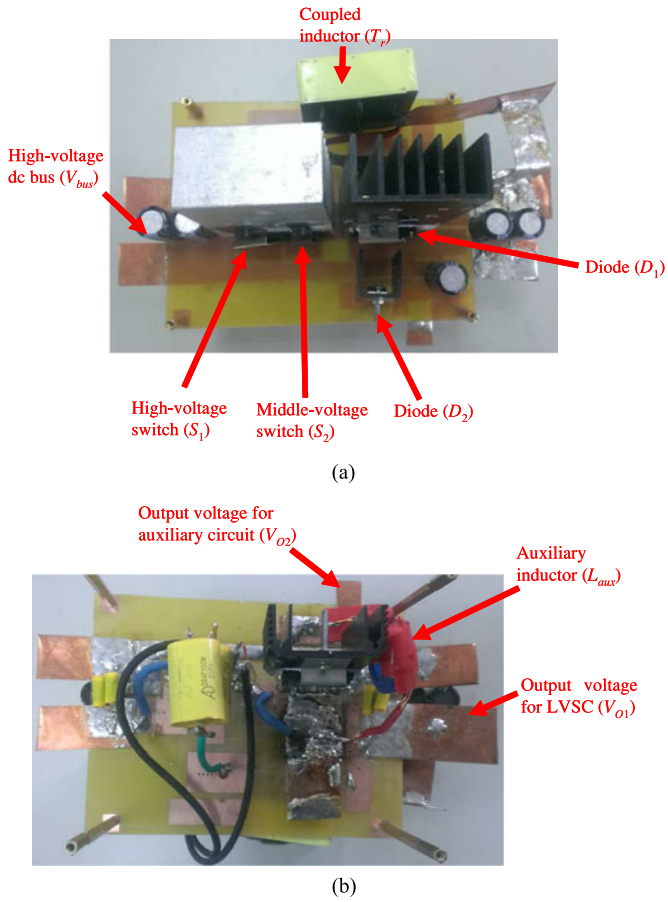

Fig. 6. Practical photograph of SIMO step-down converter: (a) front side; (b) reverse side.

In general, a 48-V voltage source generated from the ac–dc converter is used for communication systems in the network communication room [15]. Traditionally, the buck converter is used to step down the high voltage to a lower voltage. However, for the device that needs an input voltage of 3.3 V or less, an extremely low duty cycle is necessary for the buck converter if the input voltage is 48 V, thereby causing the control design to be tough and the accompanying power loss to be relatively high. In this section, one modifies the duty cycle $d_1 = 0.34$ by substituting $G_{V1} = 0.068$ and $N = 4$ into (11) for further examining the performance of the proposed SIMO step-down converter at the operational conditions of $V_{\text{bus}} = 48\,\text{V}$

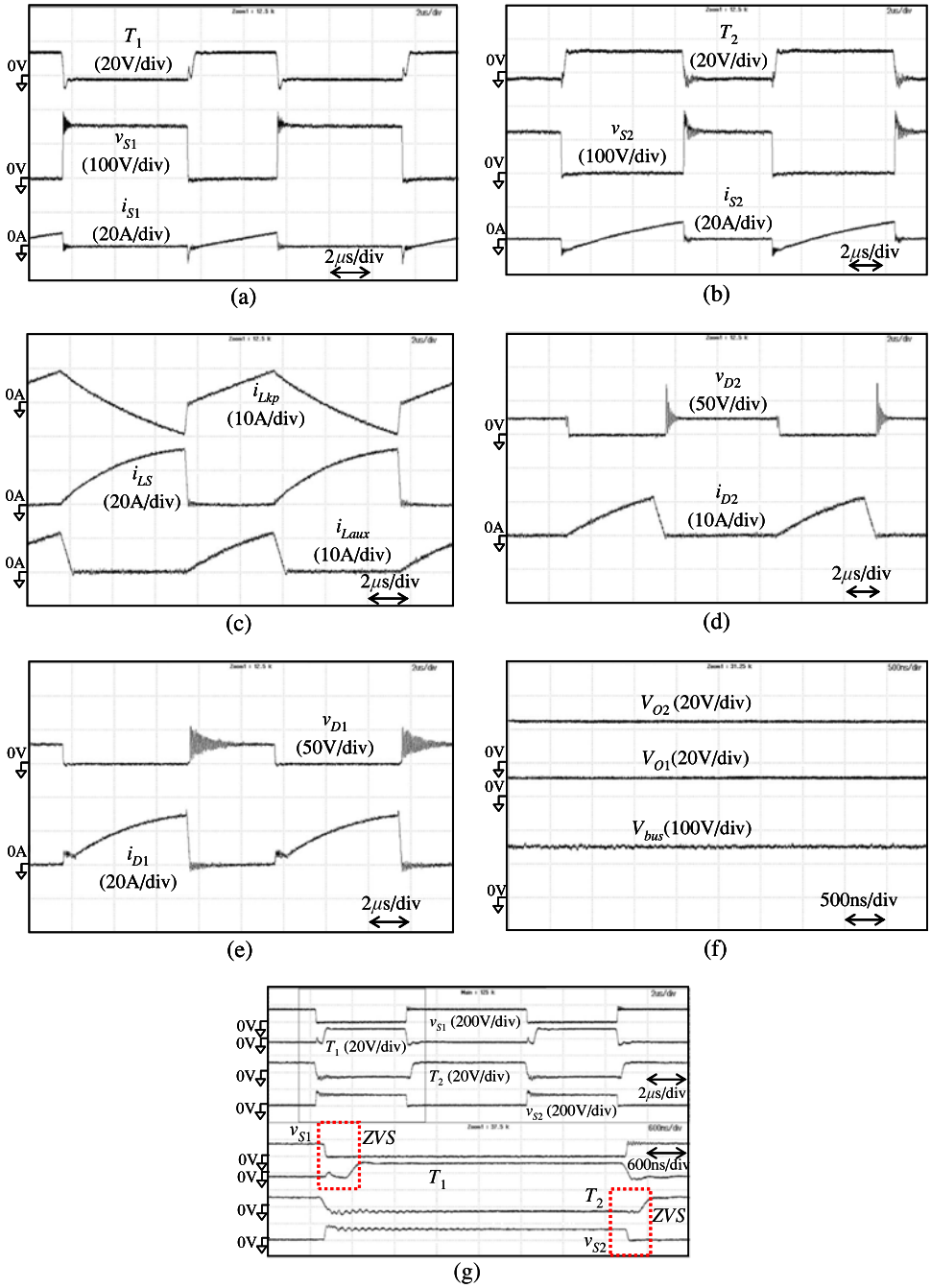

Fig. 7. Experimental voltage and current responses of SIMO step-down converter from $V_{\rm bus} = 150\,{\rm V}$ to $V_{O1} = 12\,{\rm V}$ at 15.3-A load current ($i_{O1} = 12.2\,{\rm A}$ and $i_{O2} = 3.1\,{\rm A}$).

and $V_{O1} = 3.3\,{\rm V}/V_{02} = 6-7\,{\rm V}$ Moreover, a $7.8\,\Omega$ resistor is taken as the equivalent load R_{O2} in this application. Note that, the prototype circuit of the proposed SIMO step-down converter in this alternative application is the same as Fig. 6, except for the input/output voltage and current specifications, and the corresponding duty cycle design.

A. *Experimental Results of* $V_{\rm bus} = 150\,{\rm V}/V_{O1} = 12\,{\rm V}$

The experimental voltage and current responses of the proposed SIMO step-down converter from $V_{\rm bus} = 150\,{\rm V}$ to $V_{O1} = 12\,{\rm V}$ at load currents of 15.3 A ($i_{O1} = 12.2\,{\rm A}$ and $i_{O2} = 3.1\,{\rm A}$) and 48 A ($i_{O1} = 45\,{\rm A}$ and $i_{O2} = 3\,{\rm A}$) are depicted in Figs. 7 and 8, respectively. In the subfigures (a) and (b), the trigger signals and voltage/current waveforms for the high-voltage switch (S_1) and the middle-voltage switch (S_2) are shown. Moreover, the voltage of the middle-voltage switch (v_{S2}) is steadily clamped at 120 V. As can be seen from the subfigure (c), the primary leakage current (i_{Lkp}) and the secondary inductor current (i_{Ls}) of the coupled inductor change by turns, and the charge and discharge current ($i_{L\rm aux}$) of the auxiliary inductor is the same as the analytical result in Fig. 3. In the subfigures (d) and (e), the

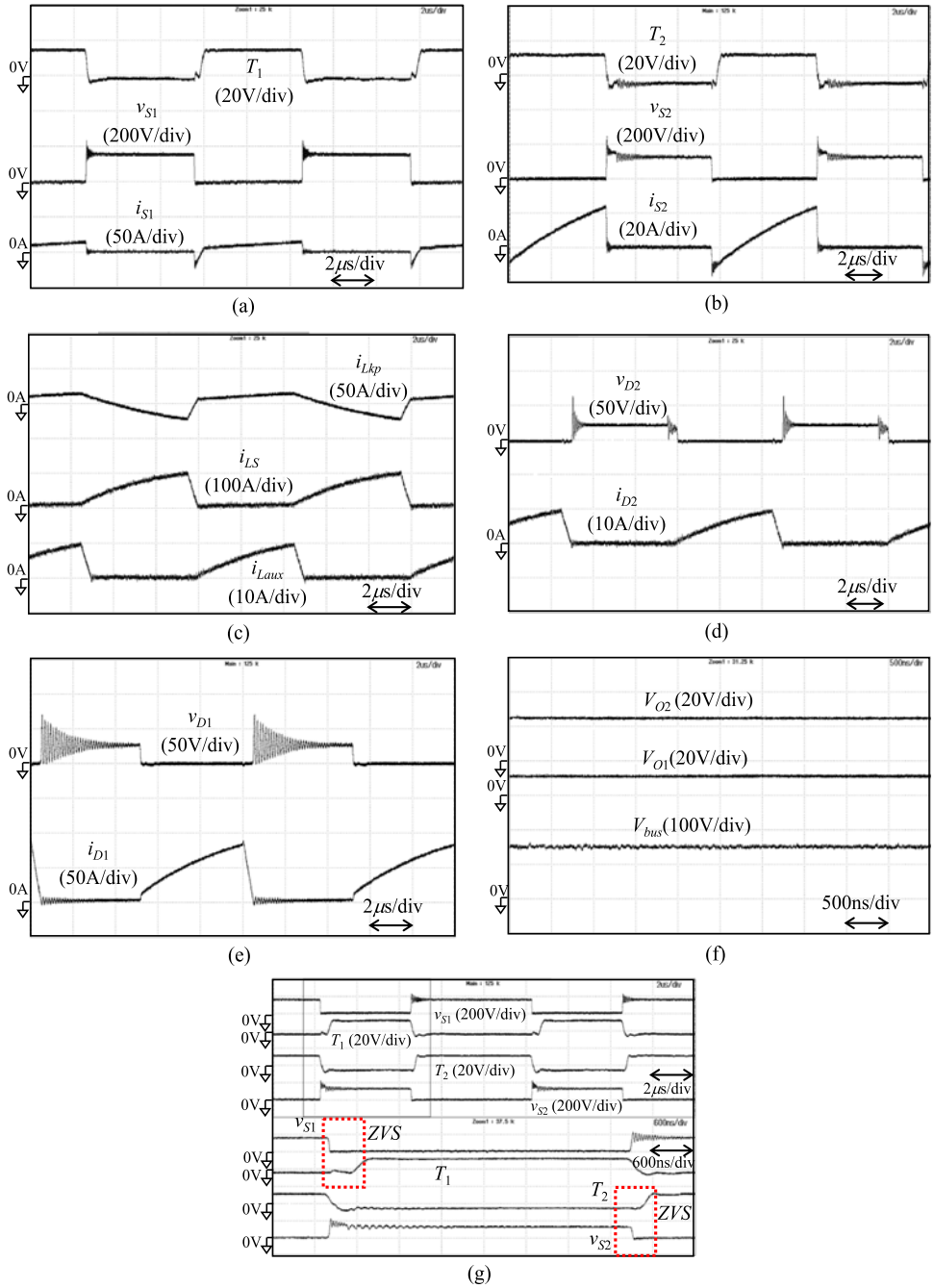

Fig. 8. Experimental voltage and current responses of SIMO step-down converter from $V_{\rm bus} = 150$V to $V_{O1} = 12$V at 48-A load current ($i_{O1} = 45$ A and $i_{O2} = 3$ A).

reverse-recovery currents can be alleviated owing to the selection of Schottky diodes for the diodes (D_1 and D_2). Note that, the voltage spikes and oscillations in the measured waveforms of v_{D1} and v_{D2} are mainly caused by the resonant phenomena between the circuit stray inductance and the parasitic capacitance of the diodes. By observing the subfigure (f), the output voltage of the LVSC can be stably adjusted by a conventional PI voltage controller to be $V_{O1} = 12$ V when the input voltage of the HVSC is $V_{\rm bus} = 150$ V. In addition, the output voltage (V_{O2}) in the auxiliary circuit does not exceed the maximum floating charge voltage of the battery module. The trigger signals and switch voltage waveforms of the high-voltage switch (S_1) and the middle-voltage switch (S_2) are enlarged in the subfigure (g). The switches of S_1 and S_2 turned ON under the condition of ZVS are obvious. The aforementioned experimental results agree well with those obtained from theoretical analyses given in Section II.

The experimental response of the proposed SIMO step-down converter from $V_{\rm bus} = 150$ V to $V_{O1} = 12$ V under the condition of load change is depicted in Fig. 9. As can be seen from

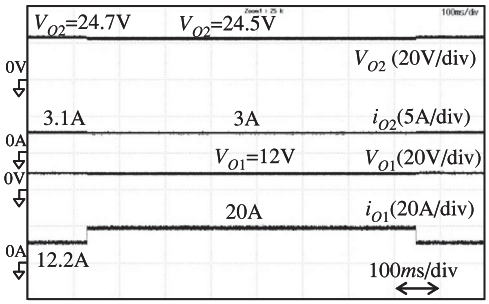

Fig. 9. Experimental response from $V_{\rm bus} = 150\,{\rm V}$ to $V_{O1} = 12\,{\rm V}$ under load current variation between $i_{O1} = 12.2\,{\rm A}$ and $i_{O1} = 20\,{\rm A}$.

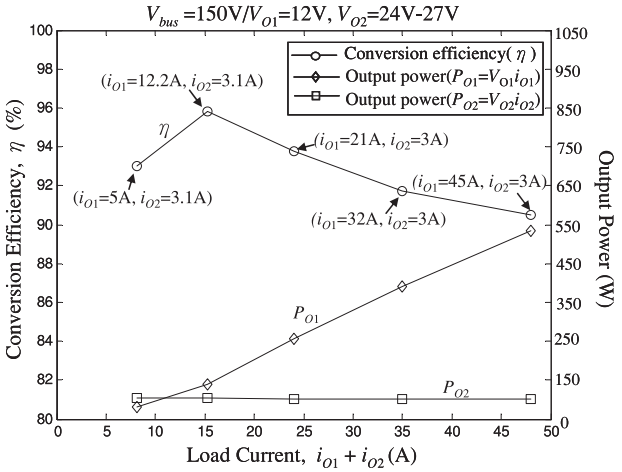

Fig. 10. Power conversion efficiency of SIMO step-down converter from 150 V to 12 V/24–27 V under different load currents.

Fig. 9, the output voltage of the LVSC can be stably controlled to be $V_{O1} = 12\,{\rm V}$ under the load current variation between $i_{O1} = 12.2\,{\rm A}$ and $i_{O1} = 20\,{\rm A}$ owing to the PI closed-loop voltage control. The output voltage of the auxiliary circuit (V_{O2}) just changes slightly from $V_{O2} = 24.7\,{\rm V}$ to $V_{O2} = 24.5\,{\rm V}$, and its voltage still does not exceed the maximum floating charge voltage of the battery module. Fig. 10 summarizes the conversion efficiency of the proposed SIMO step-down converter from $V_{\rm bus} = 150\,{\rm V}$ to $V_{O1} = 12\,{\rm V}/V_{02} = 24 - -27\,{\rm V}$ under different load currents ($i_{O1} + i_{O2}$). The conversion efficiency (η) of the proposed SIMO step-down converter is defined as the output power dividing by the input power as follows:

$$\eta = \frac{V_{O1}i_{O1} + V_{O2}i_{O2}}{V_{\rm bus}i_{\rm bus}} \equiv \frac{P_{O1} + P_{O2}}{V_{\rm bus}i_{\rm bus}} \tag{31}$$

where $V_{\rm bus}$ ($i_{\rm bus}$) and V_{O1} (i_{O1}) denote the voltages (currents) of the input power source and the output terminal at the HVSC and LVSC, respectively; V_{O2} and i_{O2} are the output voltage and current in the auxiliary circuit; $P_{O1} = V_{O1}i_{O1}$ and $P_{O2} = V_{O2}i_{O2}$ are the output powers of the LVSC and the auxiliary circuit, respectively. On the experimental system, the converter efficiency is evaluated via Power Analyzer PA4400A equipment, manufactured by the AVPower Company. The bandwidth of the PA4400A is dc to 500 kHz, and the accuracy of the measured power is within $\pm 0.1\%$. From the experimental results in Fig. 10, the average conversion efficiency of the proposed SIMO step-down converter is over 90%, and its maximum efficiency is 95.8% at the 15.3-A load current ($i_{O1} = 12.2\,{\rm A}$ and $i_{O2} = 3.1\,{\rm A}$). As a result, the objective of high-efficiency power conversion can be achieved by the proposed SIMO step-down converter.

B. Experimental Results of $V_{\rm bus} = 48\,{\rm V}/{\rm V}_{01} = 3.3\,{\rm V}$

The experimental voltage and current responses of the proposed SIMO step-down converter from $V_{\rm bus} = 48\,{\rm V}$ to $V_{O1} = 3.3\,{\rm V}$ at load currents of 3.15 A ($i_{O1} = 2.3\,{\rm A}$ and $i_{O2} = 0.85\,{\rm A}$) and 9.19 A ($i_{O1} = 8.35\,{\rm A}$ and $i_{O2} = 0.84\,{\rm A}$) are depicted in Figs. 11 and 12, respectively. In the subfigures (a) and (b), the trigger signals and voltage/current waveforms for the high-voltage switch (S_1) and the middle-voltage switch (S_2) are shown. Moreover, the voltage of the middle-voltage switch (v_{S2}) is steadily clamped at 38 V. As can be seen from the subfigure (c), the primary leakage current (i_{Lkp}) and the secondary inductor current (i_{Ls}) of the coupled inductor change by turns, and the charge and discharge current ($i_{L\rm aux}$) of the auxiliary inductor is the same as the analytical result in Fig. 3. In the subfigures (d) and (e), the reverse-recovery currents can be alleviated owing to the selection of Schottky diodes for the diodes (D_1 and D_2). Note that, the voltage spikes and oscillations in the measured waveforms of v_{D1} and v_{D2} are mainly caused by the resonant phenomena between the circuit stray inductance and the parasitic capacitance of the diodes. By observing the subfigure (f), the output voltage of the LVSC can be stably adjusted by a conventional PI voltage controller to be $V_{O1} = 3.3\,{\rm V}$ when the input voltage of the HVSC is $V_{\rm bus} = 48\,{\rm V}$. In addition, the output voltage (V_{O2}) in the auxiliary circuit is about 6.7 V. The trigger signals and switch voltage waveforms of the high-voltage switch (S_1) and the middle-voltage switch (S_2) are enlarged in the subfigure (g). The switches of S_1 and S_2 turned ON under the condition of ZVS are obvious.

The experimental response of the proposed SIMO step-down converter from $V_{\rm bus} = 48\,{\rm V}$ to $V_{O1} = 3.3\,{\rm V}$ under the condition of load change is depicted in Fig. 13. As can be seen from Fig. 13, the output voltage of the LVSC can be stably controlled to be $V_{O1} = 3.3\,{\rm V}$ under the load current variation between $i_{O1} = 2.3\,{\rm A}$ and $i_{O1} = 5\,{\rm A}$ owing to the PI closed-loop voltage control. The output voltage of the auxiliary circuit (V_{O2}) just changes slightly from $V_{O2} = 6.7\,{\rm V}$ to $V_{O2} = 6.6\,{\rm V}$. Fig. 14 summarizes the conversion efficiency of the proposed SIMO step-down converter from $V_{\rm bus} = 48\,{\rm V}$ to $V_{O1} = 3.3\,{\rm V}/V_{O2} = 6 - 7\,{\rm V}$ under different load currents ($i_{O1} + i_{O2}$). From the experimental results in Fig. 14, the average conversion efficiency of the proposed SIMO step-down converter is over 94%, and its maximum efficiency is 95.9% at 3.15-A load current ($i_{O1} = 2.3\,{\rm A}$ and $i_{O2} = 0.85\,{\rm A}$).

C. Performance Comparisons

The performance comparisons of the proposed SIMO step-down converter with similar researches in the announced works

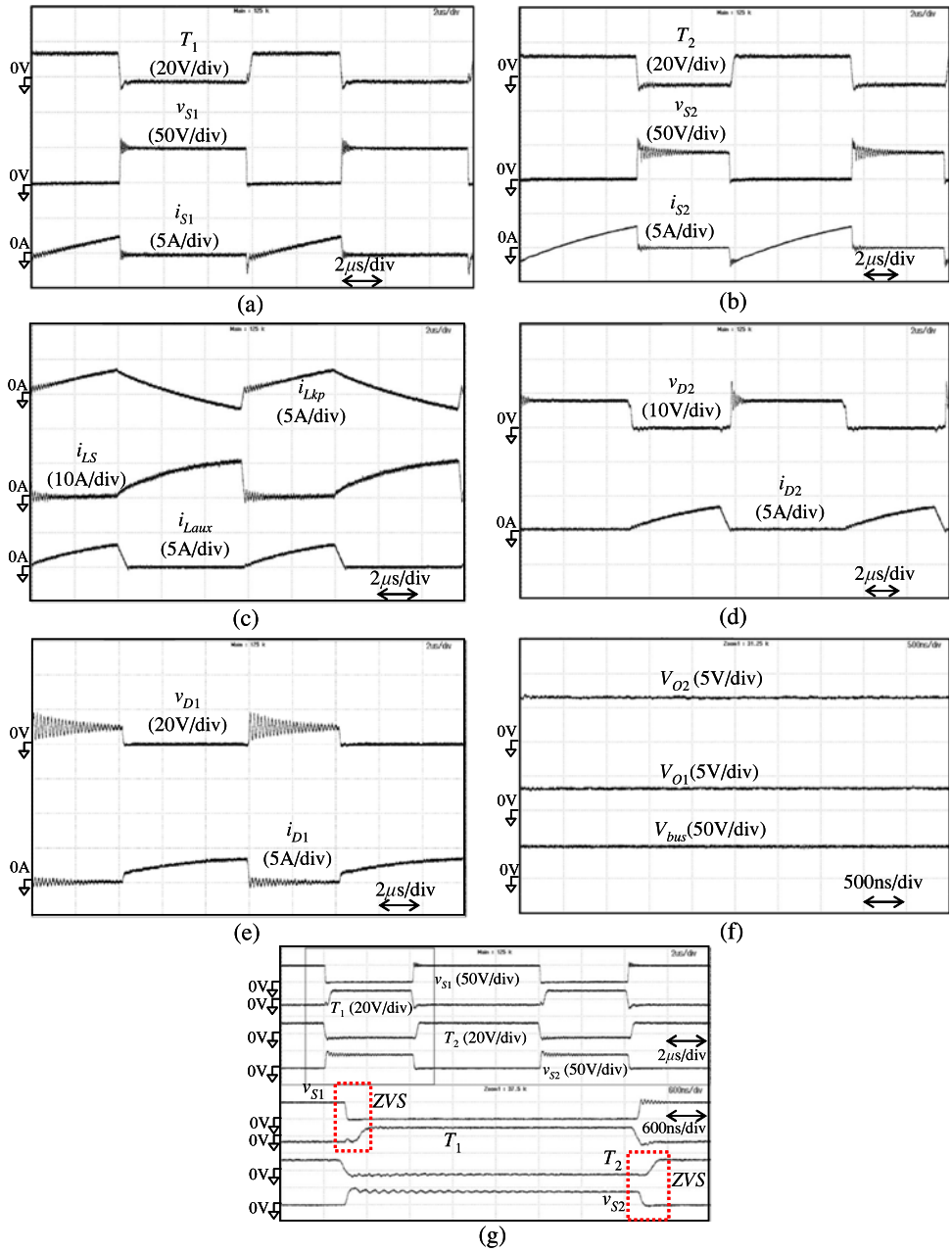

Fig. 11. Experimental voltage and current responses of SIMO step-down converter from $V_{\rm bus} = 48\,{\rm V}$ to $V_{O1} = 3.3\,{\rm V}$ at 3.15-A load current ($i_{O1} = 2.3\,{\rm A}$ and $i_{O2} = 0.85\,{\rm A}$).

[13]–[19] are summarized in Table I. The ultrahigh step-down converter presented in [15] majorly has three power switches, one coupled inductor, and one energy transferring capacitor. Although the switches (S_1 and S_2) and the diode d_1 in this study corresponds to the switches (Q_1, Q_2, and Q_3) in [15], the cost of a power MOSFET plus its driving circuit is usually higher than the diode price, and extra power for driving the power MOSFET is required. Moreover, the leakage inductance energy needs to pass through two switches in [15] for charging the energy transferring capacitor (C_B) although the function of state 2 in [15] is similar to the one of mode 3 in this study. For the same ZVS in the state 3 of [15] and the mode 4 of this study, the leakage inductance current still passes through two switches in [15]. Although the topology in [15] has the same voltage gain as the proposed SIMO step-down converter in this study, one more power switch is required in [15]. Extra conduction loss and driving power will be unavoidably occurred in [15]. In addition, the maximum voltage across the switch (Q_2) is equal to the input voltage in [15]; i.e., it has no voltage clamped function in this study. Besides, the step-down converters in [13]–[16] only have one output terminal.

As can be seen from Table I, the maximum conversion efficiency of the interleaved step-down converter in [17] is slightly higher than the one in this study. However, four power switches

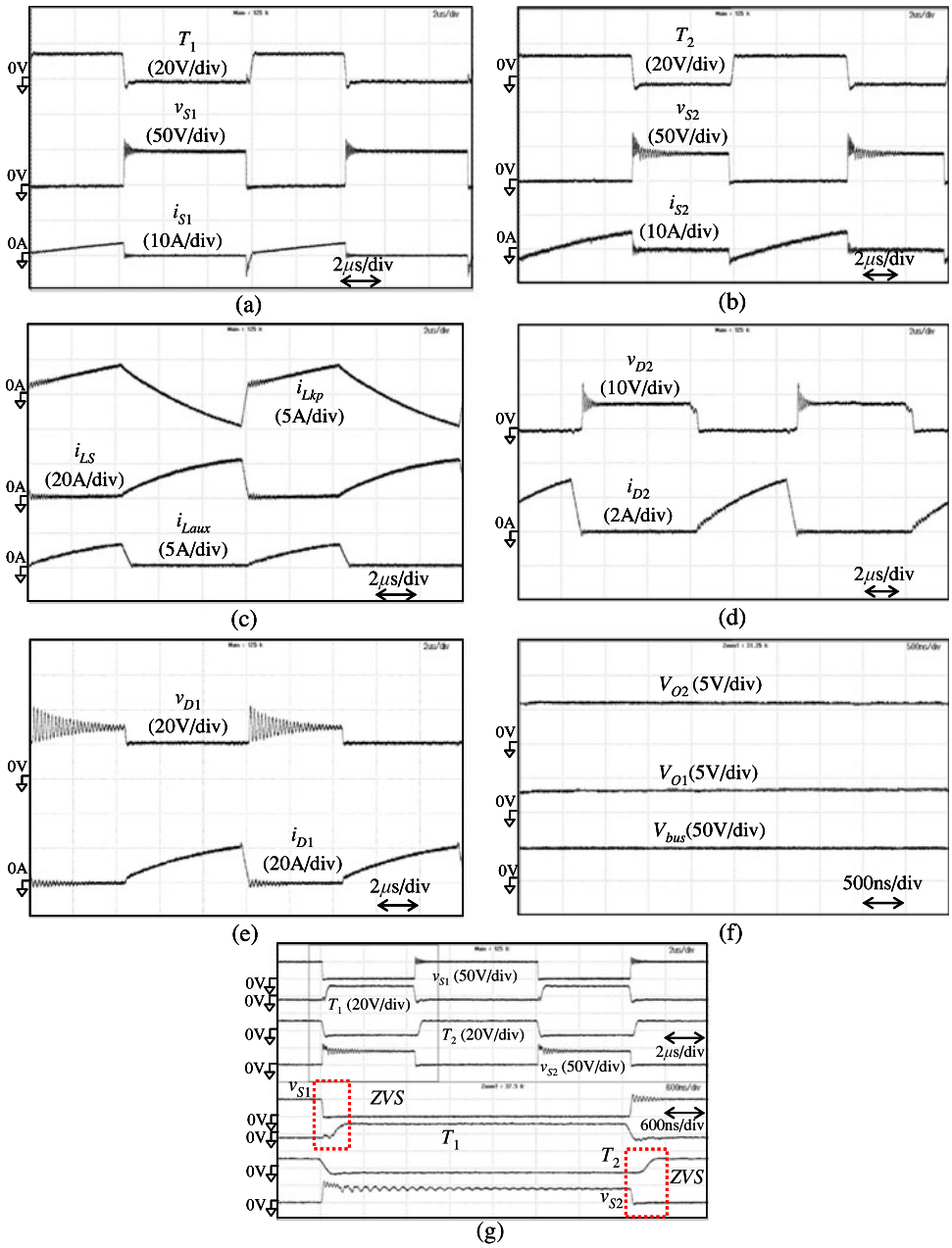

Fig. 12. Experimental voltage and current responses of SIMO step-down converter from $V_{\rm bus} = 48\,{\rm V}$ to $V_{O1} = 3.3\,{\rm V}$ at 9.19-A load current ($i_{O1} = 8.35\,{\rm A}$ and $i_{O2} = 0.84\,{\rm A}$).

are at least required for one output terminal; i.e., its manufacturing cost will be increased. For the multi-output step-down converter design, the power conversion efficiency in [18] is degenerated due to the operation of hard switching. Although there are three output terminals in [19], ten power switches are required to perform high step-down multiple output conversion. Inevitably, the control complexity and manufacturing cost of the circuit in [19] will be broadly increased. In comparison with existing works [13]–[19], the proposed SIMO step-down converter has superior properties with high conversion efficiency, high step-down ratio, low manufacturing cost, and multiple output terminals with different voltage levels.

Yau *et al.* [24] investigated a high step-down bidirectional converter utilizing four power switches, one coupled inductor, and two energy-transferring capacitors. In the step-down mode, the capacitor is connected between the input voltage and the coupled inductor, which plays a role to step down the input voltage. Although the switch (Q_3) and the capacitor (C_2) in Fig. 1 of [24] can be served as an active clamping circuit as well as another output voltage, some possible drawbacks are recited as follows: 1) the switch (Q_3) is operated at a high current spike to result in extra switching loss; 2) the capacitor (C_2) taken as the main energy storage component will be easily influenced by EMI; and 3) as can be seen from in [24, Figs. 18 and 19], the voltage clamped performance is not good.

TABLE I
PERFORMANCE COMPARISONS OF SIMO STEP-DOWN CONVERTER WITH OTHER ANNOUNCED WORKS

References	Input Voltage	Output Voltage	Major Step-Down Ratio	Output Power Examination	Maximum Conversion Efficiency	Amount of power switches	Output terminal
[13]	48 V	24 V	D	115 W	93.6%	2	1
[14]	100 V	50 V	$\frac{D+\frac{1}{N}D_x-D_a}{1+(\frac{1}{N}-1)(D_a+D_x)}$	300 W	95%	2	1
[15]	48 V	3.3 V	$\frac{D}{N+1}$	50 W	95%	3	1
[16]	150 V	24 V	$D/2$	240 W	96.25%	2	1
[17]	400 V	25 V	$D/4$	400 W	94.4 & 96.7% (synchronous rectifier)	4	1
[18]	2.4–5 V	V_1 :1.8 V V_2 : 3.3 V	D	2 W	70%	2	2
[19]	48–85 V	V_1 :10 V V_2 : 5 V V_3 : 3.3 V	N	100 W	91.5%	10	3
This study	150 V	V_1 :12 V V_2 :24 – 27V	$\frac{D}{N+1}$	612 W	95.8%	2	2
	48 V	V_1 :3.3 V V_2 :6 –7 V		32 W	95.9%		

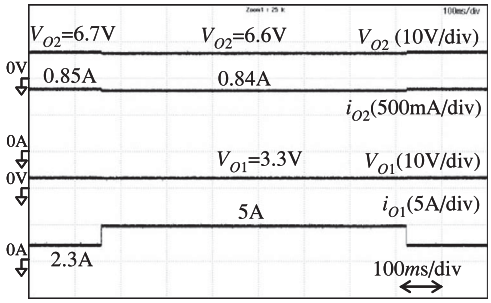

Fig. 13. Experimental response from $V_{\rm bus} = 48\,{\rm V}$ to $V_{O1} = 3.3\,{\rm V}$ under load current variation between $i_{O1} = 2.3\,{\rm A}$ and $i_{O1} = 5\,{\rm A}$.

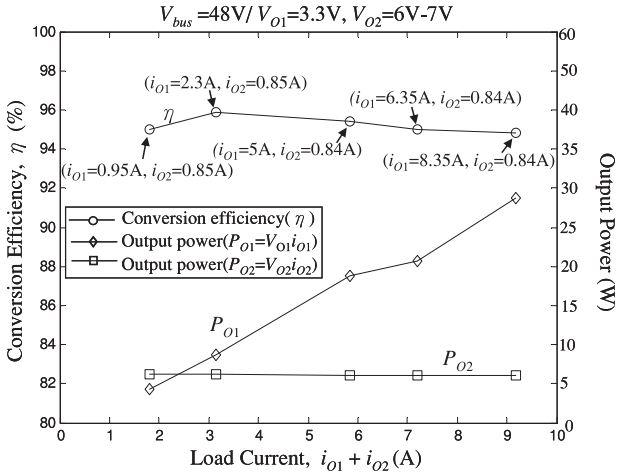

Fig. 14. Power conversion efficiency of SIMO step-down converter from 48 V to 3.3 V/6–7 V under different load currents.

V. CONCLUSION

This study has successfully developed a high-efficiency SIMO step-down converter, and this coupled-inductor-based converter was applied well to a single input power source plus two output terminals composed of an auxiliary battery module and a low-voltage load. The experimental results reveal that the maximum efficiency was measured to be 95.8%, and the average conversion efficiency was measured over 90%. The major contributions of the proposed SIMO step-down converter are recited as follows: 1) this topology adopts two power switches with the property of ZVS to achieve the objective of high-efficiency SIMO step-down power conversion; 2) the voltage ratio can be substantially increased by using a coupled inductor; 3) the stray energy can be recycled by a middle-voltage capacitor to ensure the property of voltage clamping; 4) an auxiliary inductor is designed for providing the charge power to the auxiliary battery module, and the charging voltage range can be appropriately regulated by the design of the auxiliary inductor; and 5) the copper loss in the magnetic core can be greatly reduced as a full copper film with lower turns. This high-efficiency SIMO step-down converter topology provides designers with alternative choices for stepping down a high-voltage dc bus generated by the rectifier of an ac utility power to multiple outputs with different voltage levels. The auxiliary battery module used in this study also can be extended easily to other dc loads, even for different voltage demands, via the manipulation of circuit components design.

REFERENCES

[1] L. Cao, K. H. Loo, and Y. M. Lai, "Systematic derivation of a family of output-impedance shaping methods for power converters—A case study using fuel cell-battery-powered single-phase inverter system," *IEEE Trans. Power Electron.*, vol. 30, no. 10, pp. 5854–5869, Oct. 2015.

[2] R. G. Wandhare and V. Agarwal, "Novel integration of a PV-wind energy system with enhanced efficiency," *IEEE Trans. Power Electron.*, vol. 30, no. 7, pp. 3638–3649, Jul. 2015.

[3] K. W. Hu and C. M. Liaw, "Development of a wind interior permanent-magnet synchronous generator-based microgrid and its operation control," *IEEE Trans. Power Electron.*, vol. 30, no. 9, pp. 4973–4985, Sep. 2015.

[4] F. Blaabjerg and K. Ma, "Future on power electronics for wind turbine systems," *IEEE J. Emerg. Sel. Topics Power Electron.*, vol. 1, no. 3, pp. 139–152, Sep. 2013.

[5] K. Xie, Z. Jiang, and W. Li, "Effect of wind speed on wind turbine power converter reliability," *IEEE Trans. Energy Convers.*, vol. 27, no. 1, pp. 96–104, Mar. 2012.

[6] J. Xu, S. Liao, Y. Sun, X. Y. Ma, W. Gao, X. Li, J. Gu, J. Dong, and M. Zhou, "An isolated industrial power system driven by wind coal power for aluminum productions: A case study of frequency control," *IEEE Trans. Power Syst.*, vol. 30, no. 1, pp. 471–483, Jan. 2015.

[7] F. Forest, A. T. Meynard, J. J. Huselstein, D. Flumian, C. Rizet, and A. Lacarnoy, "Design and characterization of an eight-phase-137-kW intercell transformer dedicated to multicell dc-dc stages in a modular UPS," *IEEE Trans. Power Electron.*, vol. 29, no. 1, pp. 45–55, Jan. 2014.

[8] R. Santiago Maciel, L. C. de Freitas, E. A. Alves Coelho, J. B. Vieira, and L. C. Gomes de Freitas, "Front-end converter with integrated PFC

and dc-dc functions for fuel cell UPS with DSP-based control functions," *IEEE Trans. Power Electron.*, vol. 30, no. 8, pp. 4175–4188, Aug. 2015.
[9] J. P. Rodrigues, S. A. Mussa, M. L. Heldwein, and A. J. Perin, "Three-level ZVS active clamping PWM for the dc-dc buck converter," *IEEE Trans. Power Electron.*, vol. 24, no. 10, pp. 2249–2258, Oct. 2009.
[10] Q. Du, B. Qi, T. Wang, T. Zhang, and X. Li, "A high-power input-parallel output-series buck and half bridge converter and control methods," *IEEE Trans. Power Electron.*, vol. 27, no. 6, pp. 2703–2715, Jun. 2012.
[11] L. Jiang, C. C. Mi, S. Li, C. Yin, and J. Li, "An improved soft-switching buck converter with coupled inductor," *IEEE Trans. Power Electron.*, vol. 28, no. 11, pp. 4885–4891, Nov. 2013.
[12] L. Gu, K. Jin, X. Ruan, M. Xu, and F. C. Lee, "A family of switching capacitor regulators," *IEEE Trans. Power Electron.*, vol. 26, no. 2, pp. 740–749, Feb. 2014.
[13] H. L. Do, "Zero-voltage-switching synchronous buck converter with a coupled inductor," *IEEE Trans. Ind. Electron.*, vol. 58, no. 8, pp. 3440–3447, Aug. 2011.
[14] S. S. Lee, "Step-down converter with efficient ZVS operation with load variation," *IEEE Trans. Ind. Electron.*, vol. 61, no. 1, pp. 591–597, Jan. 2014.
[15] K. I. Hwu, W. Z. Jiang, and Y. T. Yau, "Ultrahigh step-down converter," *IEEE Trans. Power Electron.*, vol. 30, no. 6, pp. 3262–3274, Jun. 2015.
[16] I. O. Lee, S. Y. Cho, and G. W. Moon, "Interleaved buck converter having low switching losses and improved step-down conversion ratio," *IEEE Trans. Power Electron.*, vol. 27, no. 8, pp. 3664–3675, Aug. 2012.
[17] C. T. Pan, C. F. Chuang, and C. C. Chu, "A novel transformerless interleaved high step-down conversion ratio dc-dc converter with low switch voltage stress," *IEEE Trans. Ind. Electron.*, vol. 61, no. 10, pp. 5290–5299, Oct. 2014.
[18] C. S. Huang, D. Chen, C. J. Chen, and K. H. Liu, "Mix-voltage conversion for single-inductor dual-output buck converters," *IEEE Trans. Power Electron.*, vol. 25, no. 8, pp. 2106–2114, Aug. 2010.
[19] H. Wu, C. Wan, W. Sun, and Y. Xing, "A high step-down multiple output converter with wide input voltage range based on quasi two-stage architecture and dual-output LLC resonant converter," *IEEE Trans. Power Electron.*, vol. 30, no. 4, pp. 1793–1796, Apr. 2015.
[20] R. J. Wai and K. H. Jheng, "High-efficiency single-input multiple-output DC-DC converter," *IEEE Trans. Power Electron.*, vol. 28, no. 2, pp. 886–898, Feb. 2013.
[21] R. J. Wai, L. S. Hong, and J. J. Liaw, "High-efficiency bidirectional single-input multiple-output power converter," *IET Power Electron.*, vol. 7, no. 5, pp. 1278–1293, May 2014.
[22] R. J. Wai and R. Y. Duan, "High step-up converter with coupled inductor," *IEEE Trans. Power Electron.*, vol. 20, no. 5, pp. 1025–1035, Sep. 2005.
[23] N. Mohan, T. M. Undeland, and W. P. Robbins, *Power Electronics: Converters, Applications, and Design*. New York, NY, USA: Wiely, 1995.
[24] Y. T. Yau, W. Z. Jiang, and K. I. Hwu, "Bidirectional operation of high step-down converter," *IEEE Trans. Power Electron.*, vol. 30, no. 12, pp. 6829–6844, Dec. 2015.

Rong-Jong Wai (M'99–SM'05) was born in Tainan, Taiwan, in 1974. He received the B.S. degree in electrical engineering and the Ph.D. degree in electronic engineering from Chung Yuan Christian University, Chung Li, Taiwan, in 1996 and 1999, respectively.

From August 1998 to July 2015, he was with Yuan Ze University, Chung Li, Taiwan, where he was the Dean of the General Affairs Office from August 2008 to July 2013, and the Chairman of the Department of Electrical Engineering from August 2014 to July 2015. Since August 2015, he has been with National Taiwan University of Science and Technology, Taipei, Taiwan, where he is currently a full Professor, and the Director of the Electric Control and System Engineering Laboratory. He is a chapter-author of *Intelligent Adaptive Control: Industrial Applications in the Applied Computational Intelligence Set* (Boca Raton, FL, USA: CRC Press, 1998) and the coauthor of *Drive and Intelligent Control of Ultrasonic Motor* (Tai-chung, Taiwan: Tsang-Hai, 1999), *Electric Control* (Tai-chung, Taiwan: Tsang-Hai, 2002) and *Fuel Cell: New Generation Energy* (Tai-chung, Taiwan: Tsang-Hai, 2004). He has authored more than 150 conference papers, more than 165 international journal papers, and 50 inventive patents. His research interests include power electronics, motor servo drives, mechatronics, energy technology, and control theory applications. The outstanding achievement of his research is for contributions to real-time intelligent control in practical applications and high-efficiency power converters in energy technology.

Dr. Wai is a Fellow of the Institution of Engineering and Technology (U.K. He received the Excellent Research Award in 2000, and the Wu Ta-You Medal and Young Researcher Award in 2003 from the National Science Council, Taiwan. In addition, he received the Outstanding Research Award in 2003 and 2007 from the Yuan Ze University, Taiwan; the Excellent Young Electrical Engineering Award and the Outstanding Electrical Engineering Professor Award in 2004 and 2010 from the Chinese Electrical Engineering Society, Taiwan; the Outstanding Professor Award in 2004 and 2008 from the Far Eastern Y. Z. Hsu−Science and Technology Memorial Foundation, Taiwan; the International Professional of the Year Award in 2005 from the International Biographical Centre, U.K.; the Young Automatic Control Engineering Award in 2005 from the Chinese Automatic Control Society, Taiwan; the Yuan-Ze Chair Professor Award in 2007, 2010, and 2013 from the Far Eastern Y. Z. Hsu−Science and Technology Memorial Foundation, Taiwan; the Electric Category-Invent Silver Medal Award in 2007, the Electronic Category-Invent Gold and Silver Medal Awards in 2008, the Environmental Protection Category-Invent Gold Medal Award in 2008, the Most Environmental Friendly Award in 2008, and the Power Category-Invent Bronze Medal Award in 2012 from the International Invention Show and Technomart, Taipei; the University Industrial Economic Contribution Award in 2010 from the Ministry of Economic Affairs, Taiwan; the Ten Outstanding Young Award in 2012 from the Ten Outstanding Young Person's Foundation, Taiwan; the Taiwan Top 100 MVP Managers Award in 2012 from MANAGER today magazine, Taiwan; the Outstanding Engineering Professor Award in 2013 from the Chinese Institute of Engineers, Taiwan, the Green Technology Category-Scientific Paper Award in 2014 from the Far Eastern Y. Z. Hsu−Science and Technology Memorial Foundation, Taiwan, and the Scopus Young Researcher Lead Award-Computer Science in 2014 from Taiwan Elsevier. His biography was listed in *Who's Who in Science and Engineering* (Marquis Who's Who) in 2004–2015, *Who's Who* (Marquis Who's Who) in 2004–2015, and *Leading Scientists of the World* (International Biographical Centre) in 2005, *Who's Who in Asia* (Marquis Who's Who), *Who's Who of Emerging Leaders* (Marquis Who's Who) in 2006–2015, and *Asia/Pacific Who's Who* (Rifacimento International) in volumes VII–XIII.

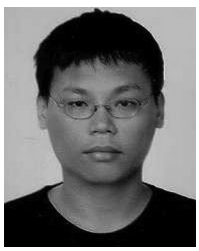

Jun-Jie Liaw was born in Yun-lin, Taiwan, in 1984. He received the B.S. degree in electronic engineering from the Kun San University of Science and Technology, Tainan, Taiwan, in 2006, and the Ph.D. degree in electrical engineering at Yuan Ze University, Chung Li, Taiwan, in 2015.

His research interests include power electronics and IC design.